Investigation of Automotive LiDAR Vision in Rain from Material and Optical Perspectives

Wing Yi Pao *, Joshua Howorth, Long Li, Martin Agelin-Chaab, Langis Roy, Julian Knutzen, Alexis Baltazar-y-Jimenez, Klaus Muenker

Posted Date: 27 March 2024

doi: 10.20944/preprints202403.1667.v1

Keywords: LiDAR; autonomous vehicle; rain; adverse weather; coating; surface wettability; optical analysis

Article

Investigation of Automotive LiDAR Vision in Rain from Material and Optical Perspectives

Wing Yi Pao [1,*], Joshua Howorth [1], Long Li [1], Martin Agelin-Chaab [1], Langis Roy [1], Julian Knutzen [2], Alexis Baltazar-y-Jimenez [3] and Klaus Muenker [4]

[1] Faculty of Engineering and Applied Science, Ontario Tech University, 2000 Simcoe St N, Oshawa, Canada
[2] Magna International, Aurora, ON, Canada
[3] Magna Exteriors, Troy, MI, USA
[4] Magna Exteriors, Sailauf, Germany
* Correspondence: wingyi.pao@ontariotechu.net

Abstract: With the emergence of autonomous functions in road vehicles, there has been an increased use of Advanced Driver Assistance Systems comprising various sensors to perform automated tasks. Light Detection and Ranging (LiDAR) is one of the most important types of optical sensor that detects the positions of obstacles, representing them as clusters of points in 3-dimensional space. LiDAR performance degrades significantly when driving in rain as raindrops adhere to the outer surface of the sensor assembly. The performance degradation behaviors include missing points and reduced reflectivity of the points. It was found that the extent of degradations is highly dependent on the interface material properties, which subsequently affects the shapes of the adherent droplets, causing different perturbations to the optical rays. A fundamental investigation is performed on the protective polycarbonate cover of the LiDAR assembly coated with four classes of materials – hydrophilic, almost-hydrophobic, hydrophobic, and superhydrophobic. Water droplets are controllably dispensed onto the cover to quantify the signal alteration due to each droplet of various sizes and shapes. To further understand the effects of droplet motion on LiDAR signals, sliding droplet conditions are simulated using numerical analysis and validated with physical optical tests using a 905 nm laser source and receiver to mimic the LiDAR detection mechanism. Comprehensive explanations are presented on LiDAR performance degradation in rain from both material and optical perspectives. These can aid component selection and the development of signal enhancing strategies for integrating LiDARs in vehicle designs to minimize the impact of rain.

Keywords: LiDAR; autonomous vehicle; rain; adverse weather; coating; surface wettability; optical analysis

1. Introduction

The development of intelligent features for road vehicles has been on the rise in recent years with a strive towards fully autonomous driving. There are five levels of autonomy defined by the Society of Automotive Engineers (SAE). Level-0 is considered to have no assistance, Level-1 offers adaptive features, Level-2 provides partial automation, Level-3 has conditional automation, Level-4 does not require driving intervention in preset environments, and Level-5 is full automation in all conditions [1]. Common Advanced Driver Assistance System (ADAS) sensors include cameras, Light Detection and Ranging (LiDARs), Radio Detection and Ranging (RADARs), and Sound Navigation and Ranging (SONARs) [2]. The sensors are responsible for perceiving environmental data and communicating with ADAS when deploying automated functions, such as emergency braking, adaptive cruise control, hands-free steering, etc.

A concern of autonomous features is the uncertainty of sensor performance degradation when driving in adverse weather conditions, particularly rain, as it is the most common precipitation form globally. Optical sensors like cameras and LiDARs are more susceptible to impairments in the rain

 doi:10.20944/preprints202403.1667.v1

due to the use of shorter wavelengths (nm-scale) which increase sensitivity to interferences. Longer wavelengths (mid and high mm-scale) sensors such as RADAR and SONAR are less prone to performance degradation as they have lower resolutions, their wavelengths are often larger than the raindrop scale (low mm-scale) [3]. On the other hand, LiDAR is a less established technology than cameras, with multiple aspects still in development, especially for automotive applications, such as electronic and photonic components, signal processing, and packaging. Therefore, this paper focuses on investigating LiDAR performance in rain.

Automotive LiDARs typically utilize the time-of-flight principle to determine the range of objects based on simple elastic scattering phenomena without wavelength changes [4]. LiDAR emits laser pulses toward a target object; the detector then calculates the time it takes to receive a backscattered signal to identify the distance of the target from the incident source. A LiDAR sends out short duration wave pulses with a known power, and the return flux is converted to an electric voltage using photodiodes or photomultipliers. The signal energy can be calculated with consideration of efficiency loss during the laser travel as stated in Equation 1 below. E, σ, A, R, and η represent energy, cross-section on the target that is illuminated, area, range, and efficiency, respectively.

$$E_{signal} = E_{transmitted} \cdot \frac{\sigma}{A_{illuminated}} \cdot \frac{A_{receiver}}{\pi R^2} \cdot \eta_{atmostpher}^2 \cdot \eta_{system} \quad (1)$$

Automotive applications employ near-infrared lasers with a wavelength of 905 nm or 1550 nm, which are suitable for short-ranging. The energy of a 905 nm LiDAR is lower than that of 1550 nm for eye safety [5]. 1550 nm may be sent out for a shorter duration and is less affected by background noise, however, 1550 nm is more prone to atmospheric absorptions by gas molecules [6]. The current state-of-the-art types and sensing schemes of LiDARs are reviewed and discussed in [7] on the construction and operating mechanisms.

From a practical point-of-view, it is desired to protect the ADAS sensors from harsh driving environments that may damage the sensor lenses due to soiling (surface contamination [8]). Thus, it has been proposed that protective covers may be used in front of the sensors with various coatings to achieve properties such as water repelling, anti-abrasion, and anti-reflection [9]. Figure 1 shows the front cover with integrated sensor modules behind.

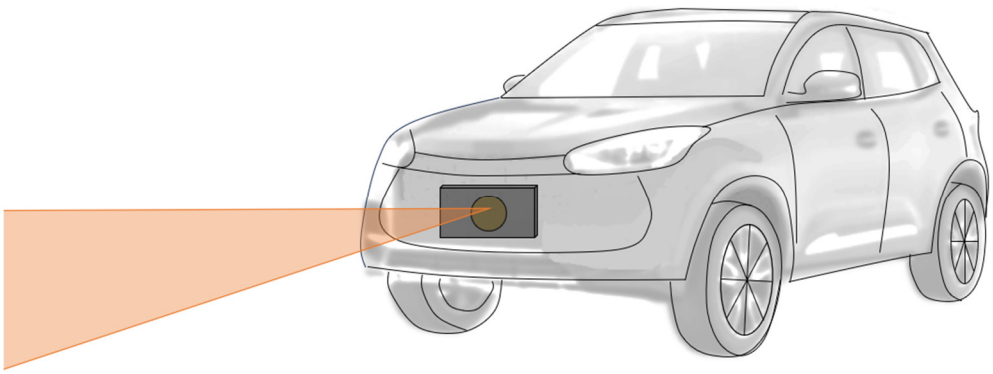

Figure 1. Demonstration of cover with integrated sensor modules behind in a vehicle.

Multiple studies suggested that LiDAR performance degrades in rain because raindrops can absorb laser energy or alter the paths of laser beams. The attenuation of light due to precipitation has been extensively studied concerning the extinction coefficients [5,10–13]; the experimental condition is demonstrated in Figure 2a for which adherent droplets on the LiDAR surface is not considered. The attenuation effect on LiDAR return signal power $P_{returned}$ is shown in Equation 2, where Z is the distance of the object from the LiDAR. The extinction coefficient ζ, is a function of natural rain intensity (I [mm·h^{-1}]) and follows a power law relationship. In Equation 3, c_1 and c_2 are constant values

 doi:10.20944/preprints202403.1667.v1

which can be determined through physical experiments. Assuming the only variable is rainfall rate, then the higher the rain intensity, the lower the return power.

$$P_{returned} \propto e^{-2\xi Z} \quad (2)$$

$$\zeta = c_1 I^{c_2} \quad (3)$$

Although the attenuation model provides an estimation of the LiDAR performance with respect to raindrop size distribution and intensity, there are other crucial factors to consider when driving in rain. Adherent raindrops are much closer to the LiDAR surface, causing obstruction and deflection of signals [14], the scenario is demonstrated in Figure 2b. Small apertures of the micro-electromechanical systems (MEMS) mirror with only a few millimeters restrict the size of the scanning laser beam, which is one of the major reasons obstructing LiDAR vision when raindrops of similar size as the aperture adheres on the outer surface of the LiDAR sensor [15]. The influence of aperture size is also discussed in [16,17]; generally, a larger aperture that can scan rapidly at a higher frequency is desired.

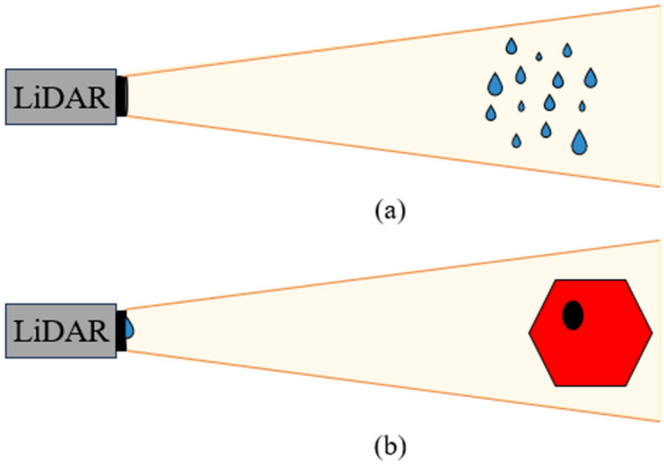

Figure 2. (**a**) LiDAR sees raindrops in mid-air which causes signal attenuation effects; (**b**) LiDAR sees raindrops adhering to the external surface of the sensor assembly which causes signal deflection and obstruction effects.

LiDAR performance degradation has also been studied on outer covers with the addition of mechanical damages and surface contaminations that are located near the LiDAR aperture [18,19]. Their studies showed that scratches on the cover affected the detection accuracy on a known position of the target. In contrast, extremely tiny droplets from dew can cause complete blindness and reduced number of points on the target when there are larger droplets present. Another recent work also reported missing measurements of LiDAR signals when exposed to rain [20]. These studies provided insights into the modes of detection faults from several possible realistic scenarios but did not investigate in depth the causes of LiDAR performance degradation. Understanding the problem fundamentally has a higher potential to allow developments for preventive measures, such as appropriate cover material and LiDAR optical component designs.

With the evolution of ADAS sensors implementations, surface coatings are no longer only considered for overall body panel protection, but also for the transmittance quality of sensor signals [21]. The size ratio between the contacting adherent raindrop and the aperture is dependent on surface material properties, which subsequently affect the raindrop impacting characteristics and dynamics at the surface such as adhesion, motion, contacting area, and shape. Surface wettability is often classified as hydrophilic, hydrophobic, and superhydrophobic when the static water contact angles (WCAs) are < 90°, between 90° – 150°, and > 150°, respectively. The resultant WCA due to surface roughness is summarized in [22] with a review of electrodeposition coatings. The method to evaluate surface wetting and droplet adhesion forces in summarized in [23] using a microbalance. Droplet impacting dynamics are affected by surface wettability, resulting in different modes of

 doi:10.20944/preprints202403.1667.v1

motion, such as sliding, rolling, bouncing, splashing, and spreading [24–26]. Recently, there have been several works reporting the tuning of wettability gradient [27] and patterning hydrophobic/hydrophilic (biphilic) properties [28] to induce droplet movements; these could be an interesting research direction in coatings for ADAS sensor applications and strategies to passively mitigate raindrops via facilitating water drainage. The droplet dynamics phenomena are expected to become more significant in driving scenarios with vehicle speed.

Our previous works show the surface material dependence during exposure to controlled and realistic simulated rain perceived by a moving vehicle [29,30], for which the use of different covers and coatings affects optical sensor visibility of the detection target at a given condition. Sample images collected in simulated realistic rain perceived by a driving vehicle are shown in Figure 3 to demonstrate the significance of cover material in LiDAR performance; the controlled rain testing method using the wind tunnels at the Automotive Centre of Excellence (ACE) at Ontario Tech University, Canada is outlined in detail in [29,30].

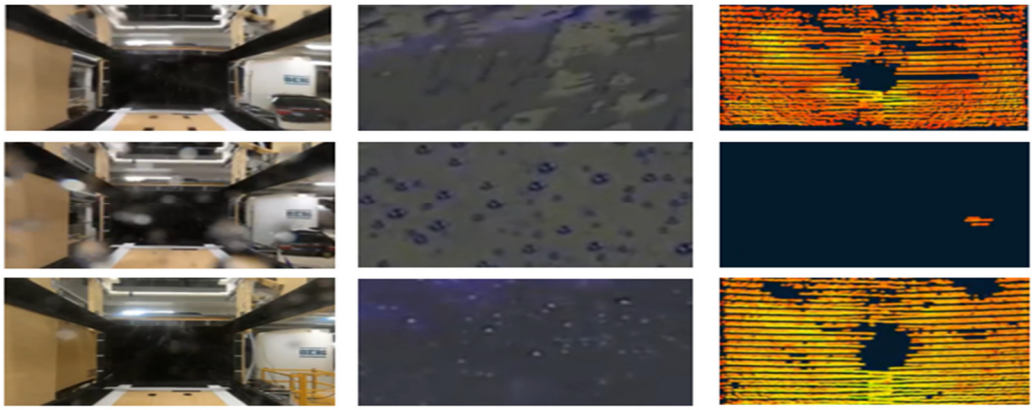

Figure 3. A matrix showing sample images of behind-cover camera perception, front-cover soiling behavior, and resulting LiDAR perception for hydrophilic (top), hydrophobic (middle), and superhydrophobic (bottom) covers. Soiling images are collected from wind tunnel rain tests based on the method reported in [29].

Since LiDAR is an optical sensor, it is hypothesized that adherent raindrops of different sizes and shapes act as localized lenses for the LiDAR within its field of view (FOV), influencing the optical paths. Some studies focus on the ball lens for beam coupling effect on optical paths [31,32], equivalent to an almost spherical droplet on a superhydrophobic surface. Meanwhile [16], discussed the ray tracing model for an adherent hemispherical droplet where the laser beam passes through a hydrophobic solid layer before reaching the droplet. They demonstrated that the ray deflection angle becomes more severe as the incident position is closer to the droplet curvature boundary. The droplet size factor is also investigated in their simulation and shows that there exists an optimal droplet size to laser beam diameter ratio to retain a higher percentage of return laser power. Limited conditions were investigated in their studies, therefore, the findings are not representative of a more comprehensive selection of cover materials, but provided insights for this study.

Currently, LiDAR performance degradation is not very well understood in the field of automotive applications, hindering development of autonomous vehicles and the deployment of LiDAR in exterior applications. One of the main reasons is due to the lack of adherent droplet studies, which are strongly related to the materials and optical properties of the surface. For instance, LiDAR performance for automotive applications may not always follow the behavior according to the return power estimation with respect to rain intensity, as Equations 2 & 3 do not incorporate the factors such as driving speed, droplet size, and droplet dynamics arising from cover materials.

The objective of the paper is to address the above-mentioned gaps by providing reasonings for LiDAR performance degradation through conducting a fundamental investigation with isolated droplet tests and discussing from materials and optical perspectives using four different classes of cover materials – hydrophilic, almost-hydrophobic, hydrophobic, and superhydrophobic. Focus is

 doi:10.20944/preprints202403.1667.v1

put on the effects of frontal covers on LiDAR performance when droplets are present. This work aims to contribute to modeling LiDAR performance when driving in rain and LiDAR signal enhancement with insights on material selections and strategies to mitigate sensor soiling.

2. Materials and Methods

The investigations of droplet influence on LiDAR sensor signals are categorized into three parts: cover material and optical characterizations, horizontal cover orientation with static droplet and LiDAR facing upward, and vertical cover orientation with dynamic droplet using an optical test bench and numerical simulation.

2.1. Material and Optical Characterizations

Four classes of cover materials are used in the study – hydrophilic, almost-hydrophobic, hydrophobic, and superhydrophobic. The covers are made of tinted polycarbonate and the wettability is tailored by applying hard coatings; the superhydrophobic cover has an extra layer of low surface energy thin film on top of the hard coat. The cover material properties are characterized for wettability using a sessile method [33] goniometer stage (Figure 4a) and surface morphology using white light interference (WLI) with the Profilm 3D surface profilometer. On the other hand, optical properties are characterized for transmittance and reflectance using a customized optical test bench. The characterizations are shown in Figure 4.

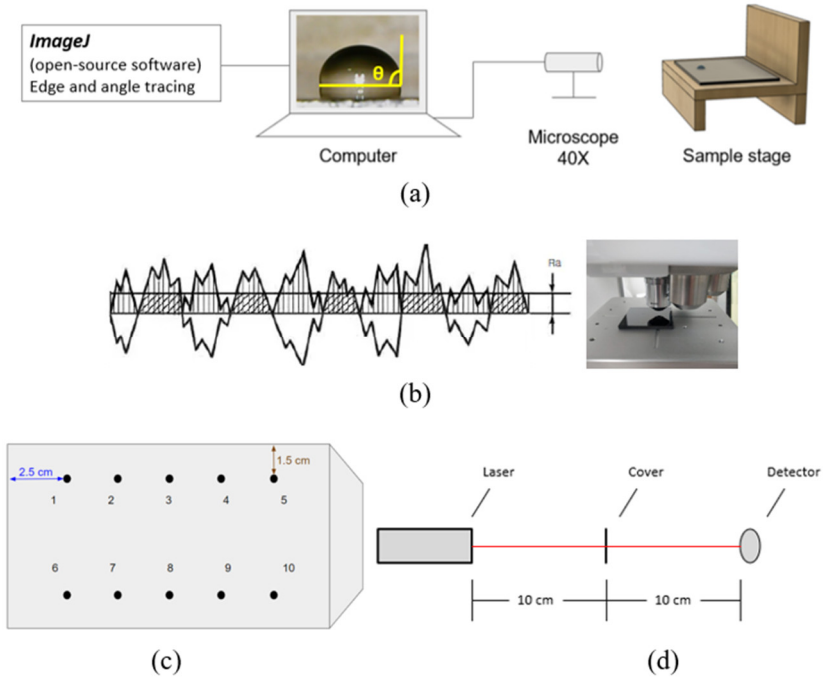

Figure 4. Characterization test benches for (**a**) static water contact angle (WCA), (**b, c**) surface roughness, and (**d**) transmittance/reflectance.

Static water contact angle (WCA) is measured using a 10 μL water droplet dispensed by a micro-pipettor. The choice of droplet volume is within the typical measurement range [34], which is similar to the size of a natural raindrop [35], as well as being controllable on a superhydrophobic surface to prevent motion. A 2-D image is taken with a 40× camera lens facing the side of the droplet, and then the WCA is calculated using a tangential line technique with the open-source ImageJ software. On the other hand, surface morphology is a factor contributing to the WCA and optical efficiency. Figure 4b explains the measurement mechanisms and roughness analysis metrics. Light waves of different wavelengths are emitted towards the cover, focusing onto an area of approximately 1 cm × 1 cm using a 20× lens; half of the beam is used as reference while the other half is for measurement. Interference occurs when the reflected and reference beams collide, causing changes in the amplitude of the

 doi:10.20944/preprints202403.1667.v1

combined wave. The interference pattern is then interpreted as roughness heights of the cover surface having peaks and troughs. For LiDAR application, cover arithmetic mean height (Sa [μm]) is the most relevant parameter to demonstrate the overall roughness profile to explain the droplet behavior and optical property, it is defined by Equation 4, which expresses the average height difference of each peak or trough compared to the surface arithmetical mean in absolute value. Both WCA and surface roughness are averaged from 10 locations on the cover, consistent with the cover manufacturing process, shown in Figure 4c.

$$Sa = \frac{1}{A}\int_A \int |Z(x,y)|dxdy \quad (4)$$

An optical test bench (Figure 4d) is customized with an aluminum platform having a series of optical components to generate a laser beam of varying wavelengths and measure its total power. Specifically, an interchangeable 905 nm laser (Laserglow Technologies, LRD-0905 Series) is used in this study, which is aligned inside the test bench to pass through a removable flat cover at a perpendicular angle. A detector is positioned at an equal distance at the other end to capture directly in the path of the laser to measure its power. The percentage of total power that transmits and reflects through the cover material is derived from the ideal situation without a cover over a range of angles of incidence between 0 – 70°. Prior to material and optical measurements, the cover sample is thoroughly cleaned with a soap solution and wiped with a microfiber cloth, except for the superhydrophobic cover which is handled carefully by rinsing with water and shake dry.

2.2. Horizontal Static Droplet Tests

A high-resolution MEMS-based forward sensing 3-D 905 nm LiDAR with linear FOV is used for the study. LiDAR signal is set to capture the first reflection mode as it is likely to be important for a vehicle to avoid the closest object rather than a stronger reflection one when navigating. The LiDAR unit is oriented facing upward with a flat surface positioned at 2.25 m from the optical center as a detection target. The LiDAR used in this study has a threshold of 10% reflectivity, points are filtered out if the signal is too weak, contributing to a small extent of uncertainty. The target detection analysis size is restricted to 0.5 m × 0.25 m of the surface, and the rest of the FOV is masked. Ten different volumes of droplets ranging from 0.5 – 30 μL are dispensed onto the cover within the 0.5 × 0.25 m custom FOV. A point cloud image is then taken, and the time gap between dispensing and image taking is kept the same as static WCA measurements to correlate droplet shape and LiDAR vision.

Visibility is defined as the area of points present and reflectivity represents the averaged signal strengths from the visible points. Visibility is measured using image processing techniques on the point cloud images. The point cloud images are converted to 8-bit grayscale with the threshold set to make the image binary, then the contours of points are mapped for area computation. Changes in visibility and reflectivity are quantified in two stages, first comparing dry LiDAR performance on the effect of cover, and second comparing LiDAR vision on the effect of a droplet on the cover. Number of points is another common method in quantifying LiDAR performance, it is usually employed for conditions that involve 3-D targets, for which it was used in our other studies [29]. But for this fundamental study, the area method is more suitable as the ground truth is a 2-D surface and evaluation of area blockage arising from the presence of a droplet is the primary interest.

2.3. Vertical Dynamic Droplet Tests

The effect of droplet sliding on optical signal is first investigated using the same optical test bench setup with the introduction of a droplet that slides down naturally due to gravity. A single 10 μL droplet is dispensed onto the cover using a micro-pipettor at a position that is just above the intersection point of the laser. As the droplet begins to slide down the cover, the percent of total power transmitted is measured with the detector in real time at 10 Hz. The procedure investigates the influence of the vertical length and curvature of a droplet on disturbances in laser transmission and the resultant transmitted power. Since the detector inside a LiDAR unit is typically positioned next to the transmitter, it is assumed that a large divergence in the laser path will result in the reflected

 doi:10.20944/preprints202403.1667.v1

signal not reaching the detector. Each case is repeated three times for hydrophilic and hydrophobic covers to obtain insights, as these are relatively controllable physical experiments compared to a non-wetting superhydrophobic cover that is only modeled numerically afterward.

While an optical test bench can provide insights into the behavior of a single laser beam in a LiDAR system in terms of signal power, it leaves questions unanswered, such as tracing the laser paths that are affected by a droplet. Therefore, the optical paths are simulated with COMSOL's optical solver, which is used to further understand the phenomena. Hypothetical droplets and water films are modeled based on images taken from different angles during wind tunnel rain experiments using the method reported in [29]. Two scenarios are studied with respect to the physical experiments: (1) simulating a single beam with droplet sliding by varying the height of the droplet while keeping the emitter and detector position constant; (2) simulating LiDAR point clouds vision by having multiple beams and a 2-D target, in this case, series of static droplets are modeled to visualize the resulting blockage behaviors. In addition to individual droplets, water film is also modeled as film formation, which is common under high droplet impact velocity and high rain intensity conditions.

3. Results

As stated earlier, the paper aims to provide some insights in LiDAR performance degradation from material and optical perspectives through correlating characterized properties, varying droplet morphology and traced laser beams. At the end of the paper, phenomenological models are proposed for the four classes of cover materials – hydrophilic, almost-hydrophobic, hydrophobic, and superhydrophobic. In this section, results are organized into four sub-sections: cover surface material properties, cover optical properties, LiDAR performance with the presence of droplets, and fundamental optical studies.

3.1. Cover Material Properties

The cover material properties are characterized comprehensively by measuring at 10 different spots on the cover, including cover thickness, surface roughness, static WCA, and the droplet thickness to contact diameter (t/D) ratio. The visuals of these properties are shown in Figure 5. These properties are hypothesized to affect LiDAR performance; the average means and standard deviations from the 10 points of measurement are reported in Table 1.

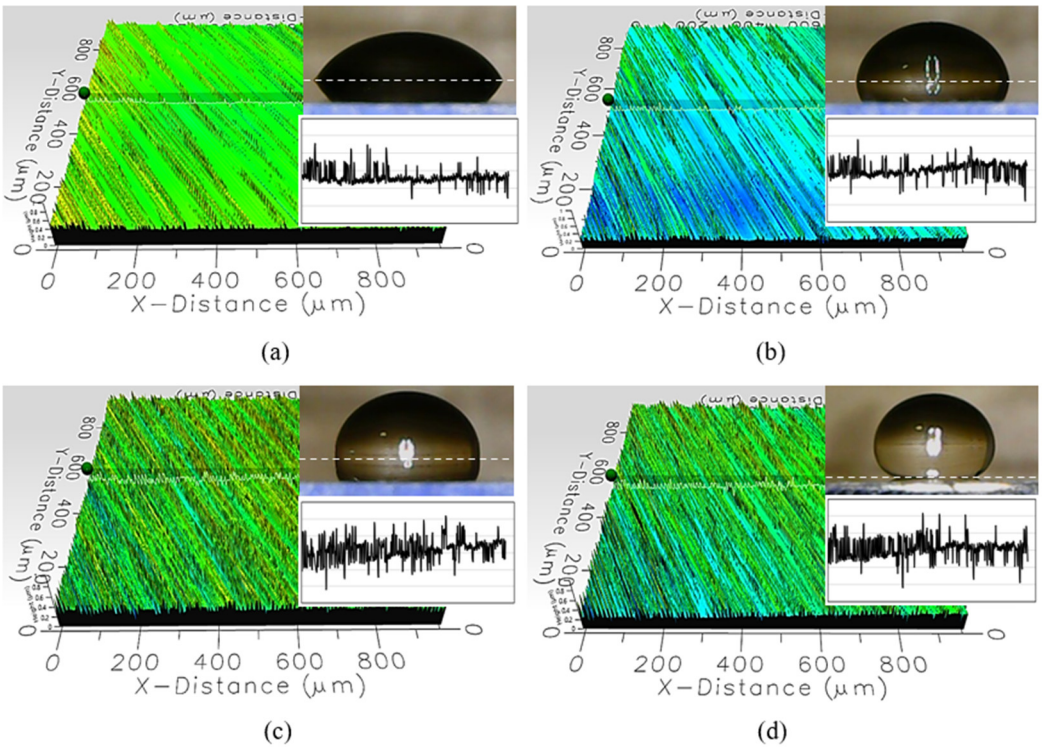

 doi:10.20944/preprints202403.1667.v1

Figure 5. Material characterizations of the (**a**) hydrophilic; (**b**) almost-hydrophobic; (**c**) hydrophobic; and (**d**) superhydrophobic covers on static water contact angle and surface roughness graphed at the same scale.

Table 1. Characterized material properties for the four classes of covers.

Cover	Cover thickness (mm)	Arithmetic mean roughness (nm)	Static WCA (deg)	t/D ratio with 15 μL droplet
Hydrophilic	2.90 ± 0.05	35.61 ± 4.42	57.08 ± 4.86	0.29 ± 0.03
Almost-hydrophobic	2.91 ± 0.03	40.05 ± 8.66	81.86 ± 2.06	0.41 ± 0.02
Hydrophobic	2.98 ± 0.01	52.31 ± 3.28	90.08 ± 0.44	0.45 ± 0.01
Superhydrophobic	3.21 ± 0.03	44.66 ± 5.42	151.95 ± 3.05	1.14 ± 0.10

Table 1 and Figure 5 suggest that the coatings are even with small standard deviations in the thickness and roughness measured over 10 different spots. The superhydrophobic cover has a low surface energy thin film on top of the hard coating; hence, it is thicker by about 0.3 mm compared to the other covers. The hydrophobic coating is the roughest, which likely has contributed to approximately 0.1 mm extra thickness compared to the hydrophilic and the almost-hydrophobic covers, considering they underwent the same coating process.

There are fewer peaks observed for the hydrophilic cover, which is also reflected in the arithmetic mean roughness that it is the smoothest among the set of covers. More rough textures with tighter gaps between the peaks are seen as the WCA increases across the set of four covers. However, with reference to the Wenzel model [36], the measured WCAs suggest that these four as-received cover coatings all have different chemical properties as they do not result in the same Young's angles after applying their respective roughness factors. This is a crucial piece of information for understanding the optical properties, as the transmittance may be affected by the material compositions in addition to thickness and surface roughness. Material compositions are not characterized in this study due to commercial restrictions.

While WCAs describe the surface wettability by classifying the overall droplet behaviors, such as droplet shape and spreading energy. To better understand the LiDAR performance from the optical perspective, wettability is quantified using a thickness to contact diameter (t/D) ratio in addition to static WCA. The main reason is due to the hypothesis that droplets are small localized lenses that change the optical path. Therefore, the curvature and contact profiles are key parameters dictating the optical paths with reference to Fresnel's equations [37] explaining transmission, reflection, and refraction.

3.2. Cover Optical Properties

The cover optical properties are characterized by transmittance (%T) and reflectance (%R) over different angles of incidence and by measuring at three different spots on the cover, labeled as Samples 1, 2, and 3 in Figure 6. As mentioned before, the cover is made of polycarbonate with coatings applied on the external surface when used with a LiDAR unit. The laser path sequence is as follows: it leaves the laser source traveling through air, then it meets the polycarbonate cover with coating on the outer side, then it travels through the air again towards the detector.

 doi:10.20944/preprints202403.1667.v1

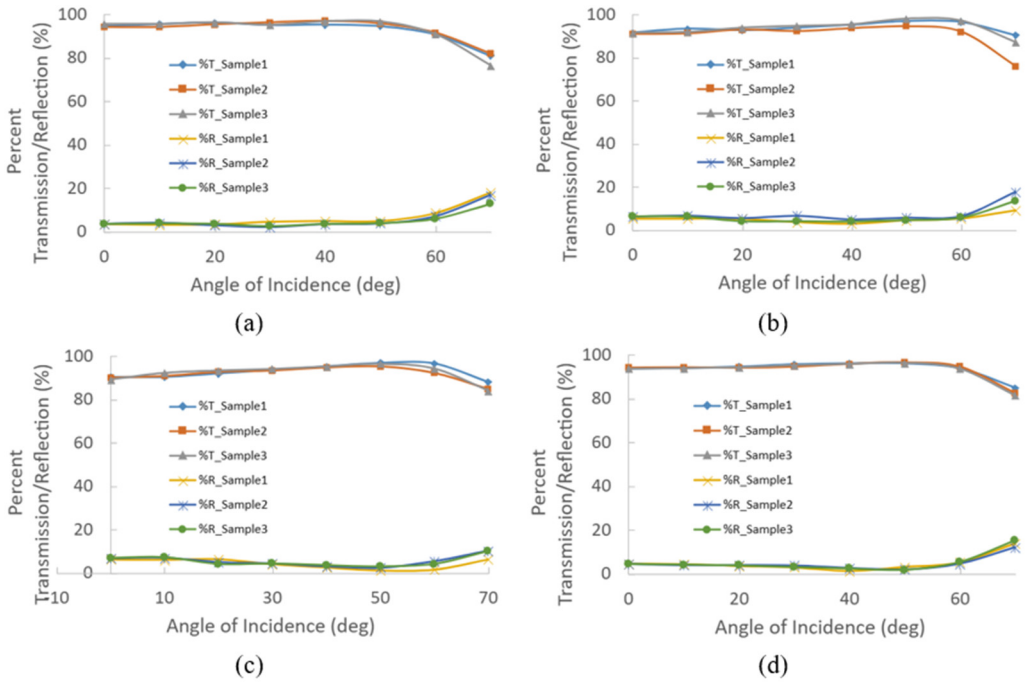

Figure 6. Transmittance and reflectance measurement for the (**a**) hydrophilic; (**b**) almost-hydrophobic; (**c**) hydrophobic; and (**d**) superhydrophobic covers using an optical test bench.

Depending on the polarization of light, whether it be unpolarized, s-polarized, or p-polarized, the amount of incident power reflected changes. Using Fresnel's equations, for p- and s-polarized lights, the total transmission decreases while reflectance increases as the angle of incidence increases between a light source and a medium. In this paper, p-polarized light is used; an anomaly is presently known as the Brewsters effect, specifically at an angle equal to the arctan of the refractive index of the second material (polycarbonate, n = 1.586) over the first material (air, n = 1). Ideally, there should be no reflection; however, in real applications, this leads to a higher transmission and lower reflection in some of the covers at around 57.7° angle of incidence for a polycarbonate material.

The refractive index changes slightly with an added thin layer of coating, which has caused differences in transmission and reflection for the four covers. The same idea can be applied for anti-reflection purposes by creating interference; the reduction in reflection will result in an increase in transmission through the material. In contrast, surface roughness may cause deviations in measurements as light is diffused away from the original position, which lowers the measured power. As mentioned in the cover material properties above, the transmittance and reflectance are affected by both surface roughness and the material composition. Although the covers cannot be directly compared, the optical results presented provide a reference on functional LiDAR covers and the recommended placement of the cover with respect to the LiDAR lens to maximize transmittance and minimize reflectance to ensure good LiDAR vision.

3.3. LiDAR Performance with the Presence of Droplets

The LiDAR visibility when using a cover is compared to the baseline without cover, reported in Table 2, which are measured to be 87.3%, 86.6%, 89.1%, and 98.8% with hydrophilic, almost-hydrophobic, hydrophobic, and superhydrophobic covers, respectively. Using a cover lowers the LiDAR visibility slightly, which aligns well with the optical property characterization. It is worth noting that laser beams emitted by the LiDAR diverge in different directions to obtain a wide FOV; thus, they are incident to the cover at different angles. As a result, the dry visibility with a flat cover parallel to the LiDAR lens is expected to differ from the optical property characterized by a single-point laser. However, the visibility should lie in between the range of transmittance measured.

 doi:10.20944/preprints202403.1667.v1

Table 2. Measured LiDAR visibility in dry condition using different covers in the sensor assembly, relative to a baseline without cover.

Cover	Visibility in dry (%)
No cover	100.0
Hydrophilic	87.3
Almost-hydrophobic	86.6
Hydrophobic	89.1
Superhydrophobic	98.8

The influence of adherent droplets on LiDAR vision is investigated with controlled single droplet tests with different droplet volumes. The presence of droplets causes missing points and it is referred to as signal blockage in Figure 7. The trend is non-linear; it could be because of several uncontrolled variables, including point cloud jittering, droplet molecular motion and spreading, droplet position, and laser beams angle of incidence within the masked FOV region to accommodate different droplet volumes. In general, however, the larger the droplet, the larger the blockage and the lower the visibility.

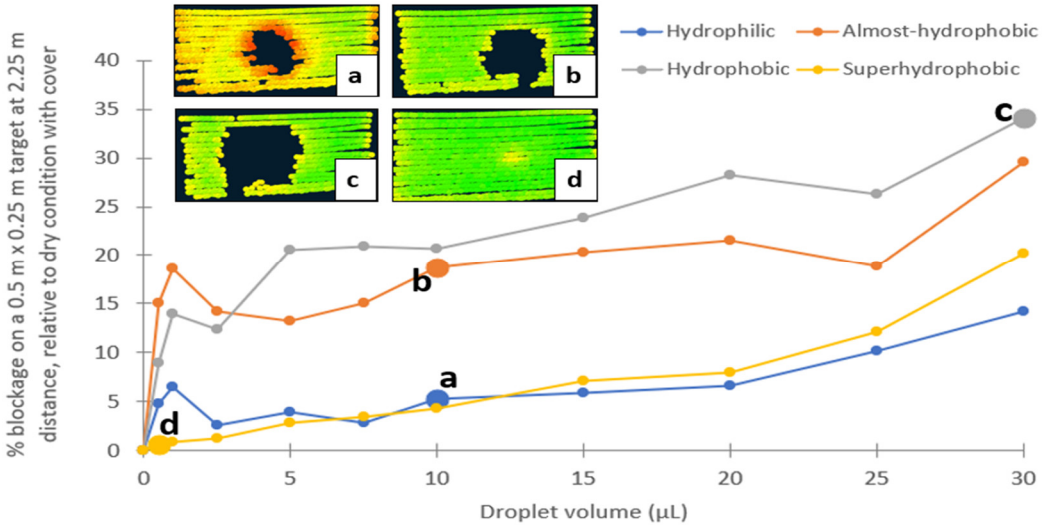

Figure 7. Percent missing point cloud (blockage) due to different droplet volumes on (**a**) hydrophilic; (**b**) almost-hydrophobic; (**c**) hydrophobic; and (**d**) superhydrophobic covers.

The rate of increase in blockage size with respect to droplet size is faster with smaller droplets on hydrophilic, almost-hydrophobic, and hydrophobic covers, this may be caused by more scattering, resulting in point cloud being less dense as partial beams are deflected. At smaller droplet sizes (≤ 2.5 µL), the blockage on the almost-hydrophobic cover is larger than that of the hydrophobic cover, likely due to the wider contact diameter from the spreading energy on the almost-hydrophobic cover while having a hemispherical shape. When the droplet volume increases (≥ 5 µL), the almost-hydrophobic cover induces more spreading and lowers the height of the droplet, which then helps to retain more visibility than a hydrophobic cover.

From the selected sample images of the blockage behavior in Figure 7, it is observed that reflectivity (signal strength) is affected, demonstrated by the change in color of the point clouds, with red having lower and green having higher reflectivity. When comparing the mean reflectivity in dry condition with the 30 µL droplet condition at points around the main blockage, the reduction in reflectivity is reported in Table 3, recorded to be 11%, 9%, 5%, and 8% for hydrophilic, almost-hydrophobic, hydrophobic, and superhydrophobic covers, respectively. Hydrophilic cover wets the most where the thinner region of the droplet is spread and resembles a water film, causing refraction and reduction in transmitted power. With less spreading, the almost-hydrophobic cover is 2% less affected than the hydrophilic cover. The hydrophobic cover generally causes missing point clouds without much effect on reflectivity changes; this is likely due to a consistent hemispherical shape

 doi:10.20944/preprints202403.1667.v1

regardless of droplet weight such that either beams are being trapped or they are extremely deflected. The superhydrophobic cover case only performs well at smaller droplet volumes and there are more partial droplet contacts due to droplet weight with larger volume, which began to have a larger effect on the laser paths.

Table 3. Measured reduction in LiDAR reflectivity in the presence of a 30 μL droplet on the cover.

Cover	Reduction in reflectivity (%)
Hydrophilic	11
Almost-hydrophobic	9
Hydrophobic	5
Superhydrophobic	8

3.4. Fundamental Optical Studies

To understand the phenomena of missing point clouds and the reduction in reflectivity due to the presence of a droplet on the cover, a droplet is dispensed physically and modeled on the cover, and allowed to slide down across the laser beam. It is found that the presence of droplets caused an obstruction to the laser signal as transmittance dropped to almost zero for most cases. Figure 8a,c shows the duration of droplet influence on optical transmittance for hydrophilic and hydrophobic covers, whereas Figure 8b,d shows the effects of droplet position and curvature on optical transmittance for almost-hydrophobic and superhydrophobic covers without considering the sliding speed. A teardrop shaped droplet slides down slower on a hydrophilic cover compared to a hemispherical droplet on a hydrophobic cover, evident by the wider trough in the transmittance curve for hydrophilic cover. This phenomenon aligns well with expectations as the hydrophobic surface is less wetting and can facilitate droplet removal faster. Whereas arbitrarily larger droplet (1.0 mm) on the almost-hydrophobic cover has a wider impact on transmittance than a smaller droplet (0.1 mm) on the superhydrophobic cover. The impact is quite symmetrical for a rounder droplet on the superhydrophobic cover. Some transmission is still permitted when the laser aligns with the center of the droplet, but the signal strength is weak, hence probably why the LiDAR point cloud shows the projected shadow of the droplet with no point cloud seen at the center when having a 10% reflectivity threshold for this LiDAR unit.

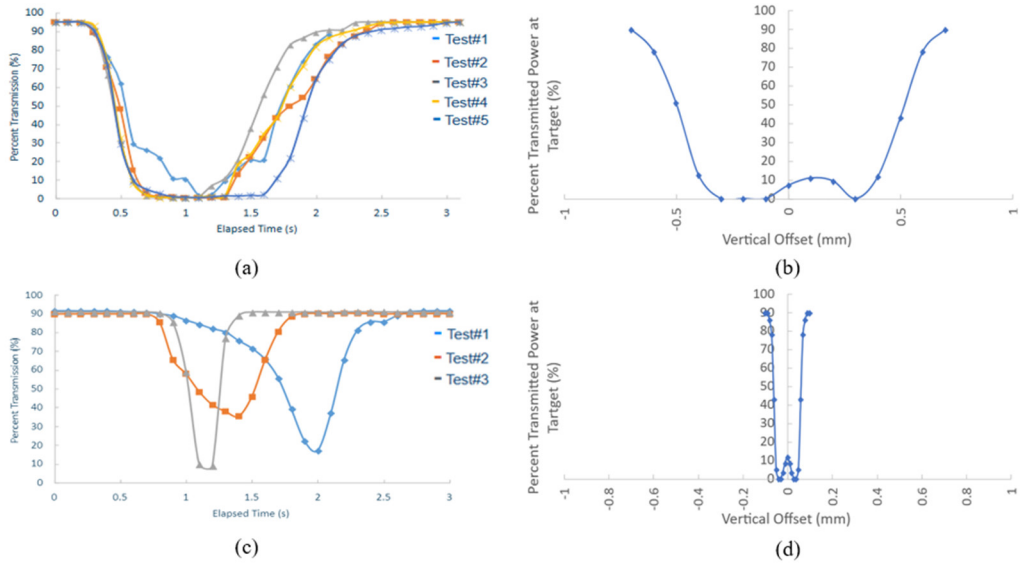

Figure 8. Influence on optical transmission due to a sliding droplet on a (**a**) hydrophilic; (**b**) almost-hydrophobic; (**c**) hydrophobic; and (**d**) superhydrophobic cover. (**a, c**) are recorded from physical experiments on duration of influence; (**b, d**) are recorded from simulation in COMSOL on the effect of position of the droplet.

 doi:10.20944/preprints202403.1667.v1

Laser beams are traced in the simulation model to visualize the weakening of signal power that results in a decrease in optical transmittance when a droplet is in the laser path. Figure 9 shows the laser paths through a hydrophobic cover towards the detector in dry and when a droplet is present at two different positions with respect to the center of the emitted laser beam. In a dry condition or no droplet (Figure 9a), most of the emitted laser power is captured by the detector on the other side, recorded to be 91% of the total power when having a 3 mm polycarbonate cover. However, when a 1 mm droplet is introduced (Figure 9b), the majority of the beam is deflected and does not reach the detector. Thus, the detected power is only 10% of the emitted power. Laser paths are observed to be sensitive to droplet position, which changes the angles of incidence at the droplet curvature. An offset of 0.1 mm (Figure 9c) of height lower than the center of the emitted laser beam further reduces the power by 5%. Therefore, it can be concluded that a droplet acts as a localized lens.

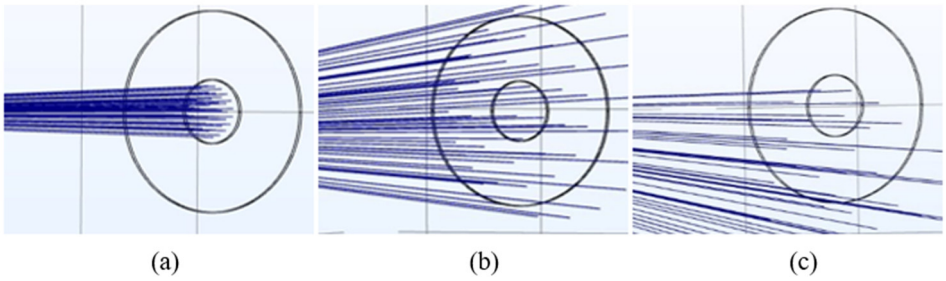

Figure 9. Laser paths for (**a**) no droplet; (**b**) a 1 mm hemispherical droplet with no position offset; and (**c**) a 1 mm hemispherical droplet with 0.1 mm position offset.

4. Discussion

4.1. Phenomenological Models

The goal of these fundamental material and optical studies is to be able to understand LiDAR vision when driving in rain. By knowing the causes of performance degradation, better strategies can be developed to mitigate the soiling effects and enhance the signals. Phenomenological models are proposed for each class of material to explain what the soiling effects would mean to LiDAR performance when driving in rain. Based on the combined effects on laser signals analyzed from the static droplet and dynamic droplet investigations, which correspond to the shape factor and time factor, respectively, the multiphase interactions are demonstrated in Figure 10. Overall, LiDAR performance degrades when adherent droplets are not removed quickly, and the direction of the originally emitted laser path changes such that fewer beams can reach the target object.

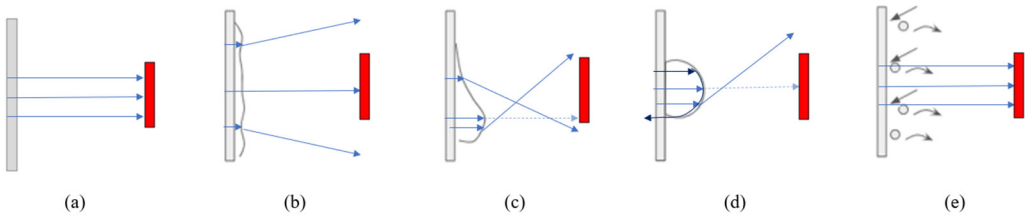

Figure 10. Phenomenological models explaining the behaviors of LiDAR laser beams for (**a**) dry condition; (**b**) hydrophilic cover with a disturbed film; (**c**) hydrophilic cover with a teardrop shaped droplet; (**d**) almost-hydrophobic/hydrophobic cover with a hemispherical droplet; and (**e**) superhydrophobic cover with non-adhering droplets.

Droplets on a hydrophilic cover have smaller blockages in general, but they affect the laser signal for longer durations as they tend to slide down slower. A hydrophilic cover, such as the one used in this study with a WCA of 57°, typically forms teardrop shaped droplets, such that there are regions of concave and convex curvatures (Figure 10c). The concave region causes laser beams to diverge, resulting in lower reflectivity at the top of the droplet. The convex region causes convergence of laser

 doi:10.20944/preprints202403.1667.v1

beams with a large extent of refraction; this results in an extremely short focal length, and the beams potentially not reaching the target. Therefore, point clouds become missing. For a more hydrophilic surface, e.g., glass with a WCA of < 25°, or at higher driving speed and rain intensity conditions, droplets spread to form a water film. A stable water film is likely to act as another smooth layer of the medium that causes a slight reduction in signal strength as the laser beams are refracted to a small degree. The thicker the water film, the further the beams deviate from the target and the lower the detected power. This may also cause a shift in the detected object position compared to the ground truth. On the other hand, a disturbed water film has ripples that randomly deflect the laser beams in all directions (Figure 10b), therefore, there is a higher chance of having missing point clouds.

Both the almost-hydrophobic and hydrophobic covers behave similar, but there is a small difference in droplet shape and dynamics arising from the 10° variance in WCA, which changes the droplet thickness to contact diameter (t/D) ratio on the cover. Droplets on the almost-hydrophobic cover have less curvature, which results in slightly smaller blockages. Both covers form almost hemispherical droplets (Figure 10d), which is the most severe LiDAR performance degradation condition. It can be explained by a combination of large refraction, weakening of laser beam falling below the LiDAR detection threshold, and total internal reflection that traps the laser beam; all of these may lead to point cloud blockages. When driving in rain, the cover experiences continuous droplet impacts; smaller droplets merge to form bigger ones and will begin to slide when the downward force exceeds the adhesion force. Normally, smaller droplets do not have enough weight to slide down quickly and tend to adhere at the same spot where the large blockages remain. Therefore, LiDAR vision is poor with these covers unless droplet drainage can be facilitated to recover the vision.

Superhydrophobic surfaces are known to be non-wetting; as such, droplets do not adhere to the cover. Droplets tend to bounce off upon impact with extremely short contact time, usually less than 20 ms [26], which is much faster than the LiDAR frame rate of ≤ 30 Hz [7]. From the optical studies, it is found that the laser beam still travels relatively straight only through the center of a curved droplet. Together with the non-wetting nature of the superhydrophobic cover which only allows adhesion of extremely small droplets, it has the advantage of maintaining straight laser paths and LiDAR vision.

4.2. Numerical Modeling of LiDAR Point Clouds

Numerical modeling is a time- and cost-efficient method to rapidly study a wide range of conditions. It is also a beneficial tool that can accelerate the advancement of ADAS and autonomous vehicles (AV) by providing a visualization and optimization platform for LiDAR vision with the presence of droplets of various sizes, shapes, concentrations, and locations. The simulated point clouds presented below can potentially revolutionize existing virtual ADAS/AV testing platforms with laser beam tracing capabilities and incorporate realistic rain influence on sensor performance due to adherent droplets on the covers.

Based on the observations of LiDAR signal blockages on the four different classes of cover materials – hydrophilic, almost-hydrophobic, hydrophobic, and superhydrophobic, the point cloud visual demonstration is extended to a superhydrophilic cover (WCA ~ 5°) that forms a complete water film, and two more hydrophilic covers (WCA ~ 25° and ~ 35°) that spread the droplets into larger localized pool, shown in Figure 11.

 doi:10.20944/preprints202403.1667.v1

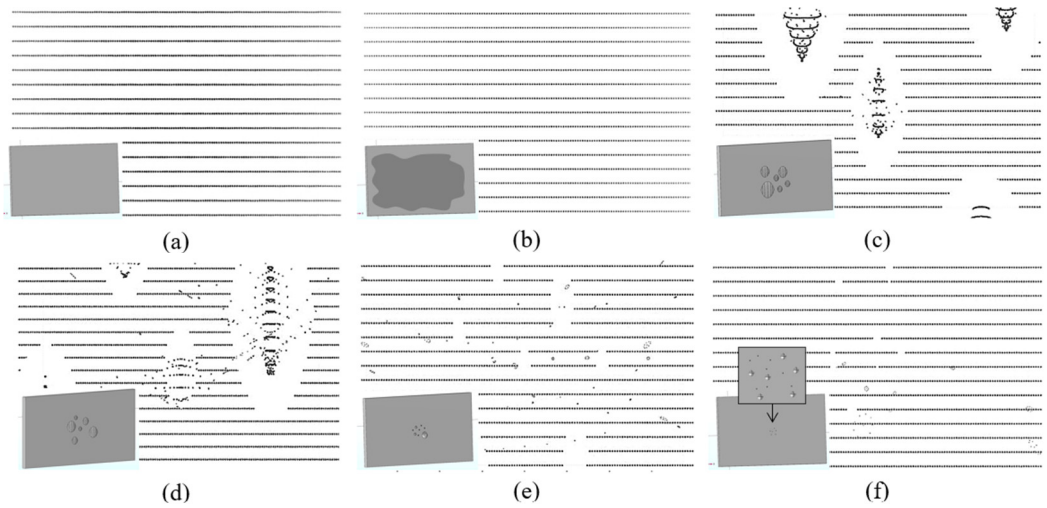

Figure 11. Simulated soiling condition and the resultant point clouds for (a) dry condition; (b) superhydrophilic cover with a stable film (WCA ~ 5°); (c) more-hydrophilic cover with large spreading droplets (WCA ~ 25°); (d) hydrophilic cover with large droplets (WCA ~ 35°); hydrophobic cover with hemispherical droplets (WCA = 90°); and (e) superhydrophobic cover with small droplets (WCA ~ 150°). Ther modeled cover and droplets are shown at the bottom left for each condition.

The superhydrophilic cover (Figure 11b) retained full visibility, but the average signal strength over the entire target is weaker than in the dry condition (Figure 11a), indicated by the lighter color of the point clouds. The two hydrophilic covers have blockages that wrap around the visible but distorted vision of the core region; this was validated by physical experiment that a larger pool of droplets results in lower reflectivity at the ring; this is because there are curvatures at the edge of the droplet while the center is relatively flat. The behaviors of the hydrophobic and superhydrophobic covers also align well with physical experiments where smaller droplets result in smaller blockages. The hydrophobic cover is seen to have some randomly distributed points; this is likely due to the refractions and shortening of focal points where false detections occur at shorter distances compared to the ground truth. This behavior was also reported in a previous work [38].

4.3. Recommendations of LiDAR Signal Enhancing Strategies

Through the comprehensive characterizations presented in this paper, several criteria for each class of cover material for maintaining LiDAR vision in rain are derived from the findings, for which they all revolve around droplet size, shape, and the dynamics:

- *Superhydrophilic cover* – stable water film, slow removal;
- *Hydrophilic cover* – medium sized droplets with low curvature, fast removal;
- *Almost-hydrophobic cover* – medium sized droplets with high spreading force.
- *Hydrophobic cover* – larger droplets to slide down with weight, fast removal without breaking the droplets into multiple smaller droplets;
- *Superhydrophobic cover* – small droplets, fast removal.

Signal enhancing strategies can be grouped into four categories – material, optical, aerodynamic, and mechanical. Examples for each category are recommended for future explorations. On the material approach, this study shows that both superhydrophobic and hydrophilic covers as a single material perform better than the almost-hydrophobic and hydrophobic ones. However, hydrophilic cover only retains LiDAR vision in lower rain intensity conditions. Patterning wettability or an electrowetting surface may be able to facilitate water drainage to prevent thick water film formation. On the optical approach, this study shows that droplets act as individual localized lenses that alter the laser paths. Therefore, compounding lenses is a potential solution to eliminate the curvature effect, however, it is a challenging task as the location of curvatures and amount of water both need to be precisely controlled. On the aerodynamic approach, cover surface morphology and orientation

 doi:10.20944/preprints202403.1667.v1

or adding air channels can be optimized to passively mitigate droplets; this method will become more effective as driving speed increases. On the other hand, active aerodynamic methods and mechanical approaches have already been commonly and extensively proposed, such as using blowers, wipers, fluid jets, and spray nozzles. To be effective, it may be beneficial to employ a hybrid approach, as each strategy has limitations and can usually only improve under limited conditions.

5. Conclusions

This paper investigates automotive LiDAR performance degradation in rain from material and optical perspectives through fundamental studies using isolated droplets and various characterizations. The work demonstrates the state-of-the-art LiDAR grade covers made of polycarbonate panel, which has good optical transmission in dry conditions at 905 nm. Four classes of cover coatings are used, including hydrophilic, almost-hydrophobic, hydrophobic, and superhydrophobic, the water contact angles (WCAs) are measured to be 57°, 82°, 90°, and 152°, respectively. The covers are further characterized by thickness, surface roughness, as well as the effect of angle of incidence on optical transmittance and reflectance to understand the property dependence of LiDAR vision.

When the LiDAR and cover assembly is exposed to a single droplet, it is observed that LiDAR performance degrades by missing point clouds or reducing signal strengths (reflectivity). The rankings of severity from the least affected to the most affected are superhydrophobic, hydrophilic, almost-hydrophobic, and hydrophobic. It seems counter-intuitive that a hydrophobic cover is an undesired approach to maintain good LiDAR vision in rain, as there are a lot of commercially available hydrophobic coating products for soiling mitigation purposes. To explain this, the optical studies suggest that a hemispherical droplet formed on the hydrophobic cover has the highest chance of not having the laser beam reach the target object due to refraction and total internal reflection, thus, translating to missing point clouds. Raindrop influence on LiDAR point clouds is numerically modeled and expanded the demonstration onto a wider spectrum of wettability, including a superhydrophilic (WCA ~ 5°) and two more hydrophilic (WCA ~ 25° and ~ 35°) covers. This paper has focused on the investigation of laser paths during the complex multiphase interactions between air, water droplets, LiDAR cover, and the optical laser beam.

In general, LiDAR performance degrades when adherent droplets are not removed quickly, and the direction of the originally emitted laser path changes such that few beams can reach the target object. This is demonstrated in the phenomenological models proposed, for which they serve as signal enhancing criteria. The material and optical analyses performed in this study provided insights into factors influencing LiDAR performance degradation. Based on the findings, several signal enhancing strategies are recommended. The current work focuses primarily on the optical path and the amount of original laser power able to reach the target object. It provides critical insights for ADAS/AV operation in terms of visibility, i.e., the ability of the vehicle to detect an obstacle. However, in future work, the distance ranging should also be investigated as it is another critical aspect for sensor perception that determines the detection accuracy.

Supplementary Materials: Not applicable.

Author Contributions: "Conceptualization, W.P., J.H., L.L., M.A., L.R., J.K., A.B. and K.M.; methodology, W.P., J.H. and L.L.; validation, W.P., J.H. and L.L.; formal analysis, W.P. and J.H.; investigation, W.P. and J.H.; resources, M.A., L.R., J.K. and A.B.; data curation, W.P. and J.H.; writing—original draft preparation, W.P. and J.H.; writing—review and editing, M.A., L.R., J.K., A.B., K.M.; visualization, W.P. and J.H.; supervision, M.A., L.R., J.K., A.B., K.M.; project administration, M.A., L.R., J.K., A.B., K.M.; funding acquisition, M.A., L.R., J.K., A.B., K.M. All authors have read and agreed to the published version of the manuscript.

Funding: Not applicable.

Institutional Review Board Statement: Not applicable.

Informed Consent Statement: Not applicable.

Data Availability Statement: The original contributions presented in the study are included in the article/supplementary material, further inquiries can be directed to the corresponding author/s.

Acknowledgments: The authors would like to acknowledge the supports from the Natural Science and Engineering Research Council of Canada (NSERC), Mitacs, the Materials Characterization Facility at Ontario Tech University, and the ACE Climatic Aerodynamic Wind Tunnel at Ontario Tech University.

Conflicts of Interest: The funders had no role in the design of the study; in the collection, analyses, or interpretation of data; in the writing of the manuscript; or in the decision to publish the results.

References

1. SAE International. Taxonomy and Definitions for Terms Related to Driving Automation Systems for On-Road Motor Vehicles. *SAE Standard* **2021**, *J3016_202104*.
2. Antony, M.M.; Whenish, R. Advanced Driver Assistance Systems (ADAS). In *Automotive Embedded Systems*. EAI/Springer Innovations in Communication and Computing; Kathiresh, M., Neelaveni, R., Eds.; Springer: Cham, Switzerland, 2021; pp. 165-181. https://doi.org/10.1007/978-3-030-59897-6_9
3. Kogut, P. Lidar vs. Radar: Differences & Uses To Pick The Right One. Available online: https://eos.com/blog/lidar-vs-radar/ (accessed on 11 Jan 2024).
4. Chazette, P.; Totems, J.; Hespel, L.; Bailly, J. 5 - Principle and Physics of the LiDAR Measurement. In *Optical Remote Sensing of Land Surface*; Baghdadi, N., Zribi, M., Eds.; Elsevier, 2016; pp. 201-247. https://doi.org/10.1016/B978-1-78548-102-4.50005-3
5. Duthon, P.; Colomb, M.; Bernardin, F. Light Transmission in Fog: The Influence of Wavelength on the Extinction Coefficient. *Applied Sciences* **2019**, 9, 2843. https://doi.org/10.3390/app9142843
6. McManamon, P.F. *Field Guide to LiDAR*; SPIE: Bellingham, USA, 2015. https://spie.org/Publications/Book/2186105
7. Li, N.; Ho, C.P.; Xue, J.; Lim, L.W.; Chen, G.; Fu, Y.H.; Lee, L.Y.T. A Progress Review on Solid-State LiDAR and Nanophotonics-Based LiDAR Sensors. *Laser Photonics Reviews* **2022**, 16, 2100511. https://doi.org/10.1002/lpor.202100511
8. Gaylard, A.P.; Kirwan, K.; Lockerby, D.A. Surface Contamination of Cars: A Review. *Journal of Automobile Engineering* **2017**, 231, pp. 1160-1176. https://doi.org/10.1177/0954407017695141
9. Pao, W.Y.; Li, L.; Agelin-Chaab, M.; Knutzen, J.; Baltazar-y-Jimenez, A. Hydrophilic Material and Coating for Automotive Lidar Sensor Covers. 2024. US20240027583A1/CA3206067A1.
10. Goodin, C.; Carruth, D.; Doude, M.; Hudson, C. Predicting the Influence of Rain on LIDAR in ADAS. *Electronics* **2019**, 8, 89. https://doi.org/10.3390/electronics8010089
11. Lewandowski, P.A.; Eichinger, W.E.; Kruger, A.; Krajewski, W.F. Lidar-based Estimation of Small-scale Rainfall: Empirical Evidence. Journal of Atmospheric and Oceanic Technology 2009, 26, pp. 656-664. https://doi.org/10.1175/2008JTECHA1122.1
12. Shah, S; Mughal, S.; Memon, S. Theoretical and Empirical Based Extinction Coefficients for Fog Attenuation in Terms of Visibility at 850 nm. In Proceedings of the International Conference on Emerging Technologies (ICET), Peshawar, Pakistan, 19-20 Dec 2015. https://doi.org/10.1109/ICET.2015.7389190
13. Byeon, M.; Yoon, S.W. Analysis of Automotive LiDAR Sensor Model Considering Scattering Effects in Regional Rain Environments. *IEEE Access* **2020**, 8, pp. 102669-102679. https://doi.org/10.1109/ACCESS.2020.2996366
14. YellowScan. Is LiDAR Compatible with Rainy or Foggy Weather? 2021. Available online: https://www.yellowscan-lidar.com/knowledge/is-lidar-compatible-with-rainy-or-foggy-weather/ (accessed on 16 Jan 2024).
15. Pacala, A. The Dead Bug Problem. Ouster. Available online: https://medium.com/ouster/the-dead-bug-problem-d80ba02127le (accessed on 16 Jan 2024).
16. Fersch, T.; Buhmann, A.; Koelpin, A.; Weigel, R. The Influence of Rain on Small Aperture LiDAR Sensors. In Proceedings of the German Microwave Conference (GeMiC), Bochum, Germany, 14-16 Mar 2016. https://doi.org/10.1109/GEMIC.2016.7461562
17. Ye, L.; Zhang, G.; You, Z. Large-Aperture kHz Operating Frequency Ti-alloy Based Optical Micro Scanning Mirror for LiDAR Application. *Micromachines* **2017**, 8, 120. https://doi.org/10.3390/mi8040120
18. Schlager, B.; Goelles, T.; Watzenig, D. Effects of Sensor Cover Damages on Point Clouds of Automotive Lidar. In Proceedings of the IEEE Sensors, Sydney, Australia, 31 Oct 2021 – 3 Nov 2021. https://doi.org/10.1109/SENSORS47087.2021.9639697
19. Schlager, B.; Goelles, T.; Muckenhuber, S.; Watzenig, D. Contaminations on Lidar Sensor Covers: Performance Degradation Including Fault Detection and Modeling as Potential Applications. *IEEE Open Journal of Intelligent Transportation Systems* **2022**, 3, pp. 738-747. https://doi.org/10.1109/OJITS.2022.3214094

20. Zhang, C.; Huang, Z.; Ang, M.H.; Rus, D. LiDAR Missing Measurement Detection for Autonomous Driving in Rain. In Proceedings of the IEEE/RSJ International Conference on Intelligent Robots and Systems (IROS), Detroit, USA, 1-5 Oct 2023. https://doi.org/10.1109/IROS55552.2023.10341932
21. Seubert, C.M. The Future of Coatings in a World of Autonomous Vehicles. CoatingsTech, 2017, 14. Available online: https://www.paint.org/coatingstech-magazine/articles/future-coatings-world-autonomous-vehicles/ (accessed on 17 Jan 2024).
22. Tam, J.; Palumbo, G.; Erb, U. Recent Advances in Superhydrophobic Electrodeposits. *Materials* **2016**, 9, 151. https://doi.org/10.3390/ma9030151
23. Law, K. Definitions for Hydrophilicity, Hydrophobicity, and Superhydrophobicity: Getting the Basics Right. Journal of Physical Chemistry Letters 2014, 5, pp. 686-688. https://doi.org/10.1021/jz402762h
24. Khodaei, M. Introductory Chapter: Superhydrophobic Surfaces – Introduction and Applications. In *Superhydrophobic Surfaces: Fabrications to Practical Applications*; Khodaei, M, Chen, X., Li, H., Eds.; IntechOpen, London, UK, pp. 1-9. https://doi.org/10.5772/intechopen.85359
25. Moghtadernejad, S; Lee, C.; Jadidi, M. An Introduction of Droplet Impact Dynamics to Engineering Students. *Fluids* **2020**, 5, 107. https://doi.org/10.3390/fluids5030107
26. Yu, X.; Zhang, Y.; Hu, R.; Luo, X. Water Droplet Bouncing Dynamics. *Nano Energy* **2021**, 81, 105647. https://doi.org/10.1016/j.nanoen.2020.105647
27. Yang, Y.; Xu, L.; Zhang, X.; Wang, S. Bioinspired Wettable-Nonwettable Micropatterns for Emerging Applications. *Journal of Materials Chemistry B* **2020**, 8, 8101. https://doi.org/10.1039/d0tb01382j
28. Nioras, D.; Ellinas, K.; Gogolides, E. Atmospheric Water Harvesting on Micro-nanotextured Biphilic Surfaces. *ACS Applied Nano Materials* **2022**, 5, pp. 11334-11341. https://doi.org/10.1021/acsanm.2c02439
29. Pao, W.Y.; Li, L.; Howorth, J.; Agelin-Chaab, M.; Roy, L.; Knutzen, J.; Baltazar-y-Jimenez, A.; Muenker, K. Wind Tunnel Testing Methodology for Autonomous Vehicle Optical Sensors in Adverse Weather Conditions. In 23. Internationales Stuttgarter Symposium; Kulzer, A.C., Reuss, H.C., Wagner, A., Eds.; Springer Vieweg, Wiesbaden, Germany, pp. 13-39. https://doi.org/10.1007/978-3-658-42236-3_2
30. Pao, W.Y.; Li, L.; Agelin-Chaab, M. Perceived Rain Dynamics on Hydrophilic/Hydrophobic Lens Surfaces and Their Influences on Vehicle Camera Performance. *Transactions of the Canadian Society for Mechanical Engineering* **2024**. https://doi.org/10.1139/tcsme-2023-0156
31. Gulari, M.N.; Tripathi, A.; Ghannad-Rezaie, M.; Chronis, N. An Optofluidic Lens Array Microchip for High Resolution Stereo Microscopy. *Micromachines* **2014**, 5, pp. 607-621. https://doi.org/10.3390/mi5030607
32. Andryieuski A.; Andryieuski, V.F. Tutorial on Optical Fiber Coupling and Bonding of Internal Parts. In *Laser Diode Module Manufacturing*; Spetz, B., Ed.; Laser Diode Source, 2021. Available online: https://www.laserdiodesource.com/Laser-Diode-Module-Manufacturing-Tutorial (accessed on 19 Jan 2024).
33. Ponomar, M.; Krasnyuk, E.; Butylskii, D.; Nikonenko, V.; Wang, Y.; Jiang, C.; Xu, T.; Pismenskaya, N. Sessile Drop Method: Critical Analysis and Optimization for Measuring the Contact Angle of an Ion-Exchange Membrane Surface. *Membranes* **2022**, 12, 765. https://doi.org/10.3390/membranes12080765
34. Huhtamaki, T.; Tian, X.; Korhonen, J.T.; Ras, R.H.A. Surface-wetting Characterization Using Contact-angle Measurements. *Nature Protocols* **2018**, 13, pp. 1521-1538. https://doi.org/10.1038/s41596-018-0003-z
35. Pao, W.Y.; Carvalho, M.; Hosseinnouri, F.; Li, L.; Rouaix, C.; Agelin-Chaab, M.; Hangan, H.; Gultepe, I.; Komar, J. Evaluating Weather Impact on Vehicles: A Systematic Review of Perceived Precipitation Dynamics and Testing Methodologies. *Engineering Research Express* **2024**, 6, 013001. https://doi.org/10.1088/2631-8695/ad2033
36. Wolansky, G.; Marmur, A. Apparent Contact Angles on Rough Surfaces: the Wenzel Equation Revisited. *Colloids and Surfaces A: Physicochemical and Engineering Aspects* **1999**, 156, pp. 381-388. https://doi.org/10.1016/S0927-7757(99)00098-9
37. Skaar, J. Fresnel's Equations in Statics and Quasistatics. *European Journal of Physics* **2019**, 40, 045201. https://doi.org/10.1088/1361-6404/ab166b
38. Pao, W.Y.; Li, L.; Agelin-Chaab, M. Wind-Driven Rain Effects on Automotive Camera and LiDAR Performances. In Proceedings of the Canadian Society for Mechanical Engineering (CSME) International Congress, Edmonton, Canada, 5-8 Jun 2022. https://doi.org/10.7939/r3-e4xk-g069